IEEE Photonics Journal
An IEEE Photonics Society Publication

Open Access

Multiple Modes-Induced Multi-Pair Cross-Phase Modulation Instability in the Deep Normal Dispersion Regime of a Tellurite High Birefringence Microstructured Optical Fiber

Volume 13, Number 1, February 2021

Tonglei Cheng
Bin Li
Xiaoyu Chen
Xin Yan
Xuenan Zhang
Fang Wang
Shuguang Li
Takenobu Suzuki
Yasutake Ohishi

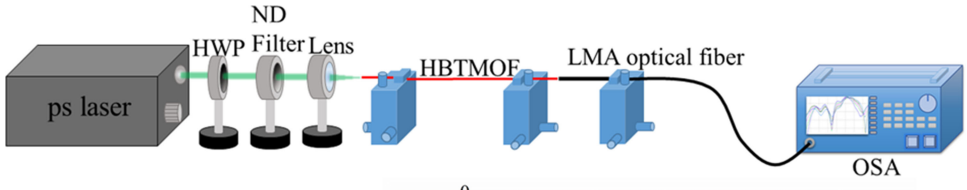

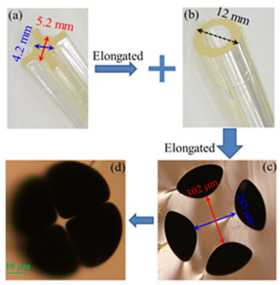

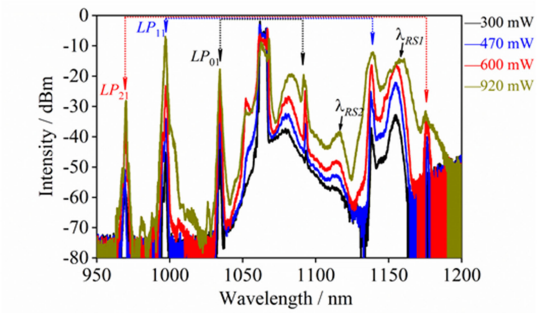

DOI: 10.1109/JPHOT.2021.3050181

Multiple Modes-Induced Multi-Pair Cross-Phase Modulation Instability in the Deep Normal Dispersion Regime of a Tellurite High Birefringence Microstructured Optical Fiber

Tonglei Cheng,[1,3] Bin Li,[1] Xiaoyu Chen,[1] Xin Yan,[1] Xuenan Zhang,[1] Fang Wang,[1] Shuguang Li,[1] Takenobu Suzuki,[2] and Yasutake Ohishi[2]

[1]State Key Laboratory of Synthetical Automation for Process Industries, College of Information Science and Engineering, Northeastern University, Shenyang 110819, China
[2]Research Center for Advanced Photon Technology, Toyota Technological Institute, Nagoya 468-8511, Japan
[3]Hebei Key Laboratory of Micro-Nano Precision Optical Sensing and Measurement Technology, Qinhuangdao 066004, China

DOI:10.1109/JPHOT.2021.3050181

Manuscript received December 7, 2020; revised December 24, 2020; accepted January 5, 2021. Date of publication January 8, 2021; date of current version January 25, 2021. This work was supported in part by the National Key Research and Development Program of China under Grant 2017YFA0701201, in part by the National Natural Science Foundation of China under Grants 61775032 and 11604042, in part by the Fundamental Research Funds for the Central Universities under Grants N180406002, N180408018, and N2004021, in part by the JSPS KAKENHI under Grants 17K18891 and 18H01504, and in part by the JSPS and CERN under the JSPS-CERN joint research program and 111 Project B16009. Corresponding author: Fang Wang (e-mail: wangfang@ise.neu.edu.cn).

Abstract: In this paper, multi-pair cross-phase modulation instability (XPMI) induced by multiple modes was experimentally observed in the deep normal dispersion regime of a tellurite high birefringence microstructured optical fiber (HBMOF) fabricated based on 76.5TeO_2-6Bi_2O_3-11.5Li_2O-6ZnO (TBLZ) glass. At the pump wavelength of 1062.7 nm three modes were emitted, whose modal birefringence was on the order of $>10^{-5}$, providing a good platform for the multi-pair XPMI generation. During the experimental investigation, a picosecond laser was adopted as the pump source, and a three-pair XPMI induced by the three modes was observed in the deep normal dispersion regime of the tellurite HBMOF. This work provide reference for the development of multi-wavelength fiber amplifiers and all-optical modulators.

Index Terms: Tellurite high birefringence microstructured optical fiber, cross-phase modulation instability, deep normal dispersion regime.

1. Introduction

Being a well-known fundamental nonlinear process, modulational instability (MI) in optical fibers refers to the exponential growth from quantum noise of symmetric sidebands around the pump which comes from the interaction between the nonlinear effect and group velocity dispersion (GVD) [1]–[5]. MI has been widely applied to fiber optical parametric oscillators (FOPOs) [6], all-optical

TABLE 1
Sellmeier Coefficients of TBLZ Glass

$$n^2(\lambda) = 1 + \sum_{i=1}^{3} \frac{A_i \lambda^2}{\lambda^2 - L_i^2}$$

i	A_i	L_i / μm
1	1.67189	0.0216
2	1.34862	0.23917
3	0.62186	6.8356

modulators [7], all-optical switching [8], fiber sources producing photon pairs [9], [10] and two-color pulses for nonlinear microscopy [11], [12], etc. The cross-phase modulation (XPM) is the coupling between two optical fields having different wavelengths or two distinct polarization modes, and under appropriate conditions it can make the two fields interact efficiently [2], [13]. XPM can induce MI in the normal GVD regime, which is called cross-phase modulation instability (XPMI), generated by coupling from cross-phase modulation of multiple beams such as stimulated Raman and sell phase modulation or Laser beam and self-modulation[14]–[18]. Due to the ability to support two orthogonal polarization states, high birefringence optical fibers (HBOFs, on the order of 10^{-5} and more) provide a good platform for generating XPMI [19]–[22]. The first observation of XPMI in the normal GVD regime of optical fibers was reported in 1988 by Baldeck [23], and since then many investigations have been carried out, mainly focusing on single pair of XPMI induced by the fundamental mode [24]–[28]. Up to now, there is no report on multi-pair XPMI induced by multiple modes in HBOFs.

Compared to the silica high birefringence microstructured optical fibers (HBMOFs), tellurite HBMOFs have high nonlinear material indices [29]–[31] which can effectively increase the fiber nonlinearity and improve MI generation. Furthermore, their high refractive-index difference between the core and cladding can increase the mode number and greatly enhance the possibility for generating multi-pair XPMI. In this paper, a tellurite HBMOF was designed and fabricated based on 76.5TeO_2-6Bi_2O_3-11.5Li_2O-6ZnO (TBLZ) glass. At the pump wavelength of 1062.7 nm three modes were emitted, whose modal birefringence was on the order of $>10^{-5}$. Using a picosecond laser as the pump source, a three-pair XPMI was obtained in the deep normal dispersion regime of the tellurite HBMOF. The multi-pair XPMI revealed in this work provide reference for the development of multi-wavelength fiber amplifiers and all-optical modulators.

2. Properties of the Tellurite HBMOF

The tellurite HBMOF was fabricated based on the TBLZ glass using the rod-in-tube drawing technique [32], [33]. The Sellmeier coefficients of TBLZ glass was shown in Table 1. The fabrication process is shown in Fig. 1. The cross-shaped rod (Fig. 1(a)) and the tube (Fig. 1(b)) were prepared by the casting method and the rotational casting method, respectively. To obtain a high birefringence feature, the mold used for making the cross-shaped rod was improved based on the one used in [Ref. 31]. Exhibiting an obvious ellipse shape (4.2 mm and 5.2 mm), the cross-shaped rod was elongated and inserted into the tube. They were further elongated to produce a preform with an ellipse shape of 245 μm and 302 μm. Finally, a 30 cm long perform was inserted into another tube to produce the tellurite HBMOF at a temperature of 307°C. During the fiber-drawing process, a positive pressure of nitrogen gas (1∼2 kPa larger than the standard atmospheric pressure) was filled into the four holes to prevent their collapse and to control the size of the core diameter. The attenuation of the tellurite fiber was ∼0.2 dB/m @1062.7 nm, which was measured by the cutback technique.

The lengths of the two principal axes of the tellurite HBMOF were respectively measured to be ∼4.6 and 3.7 μm, the difference of which helped maintain the state of linear polarization of the

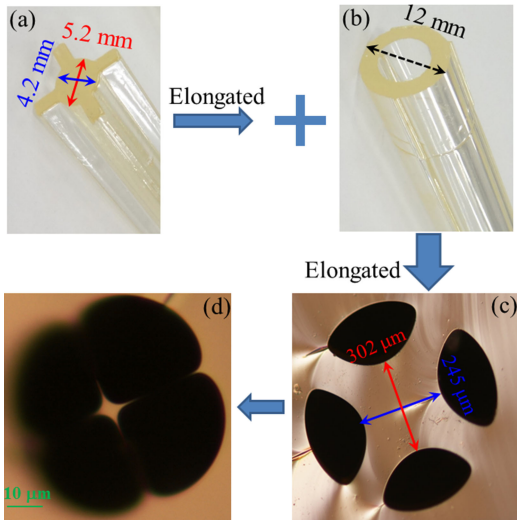

Fig. 1. Fabrication process of the tellurite HBMOF. (a) Cross-shaped rod. (b) TBLZ rod. (c) Capillary with an ellipse shape. (d) Tellurite HBMOF.

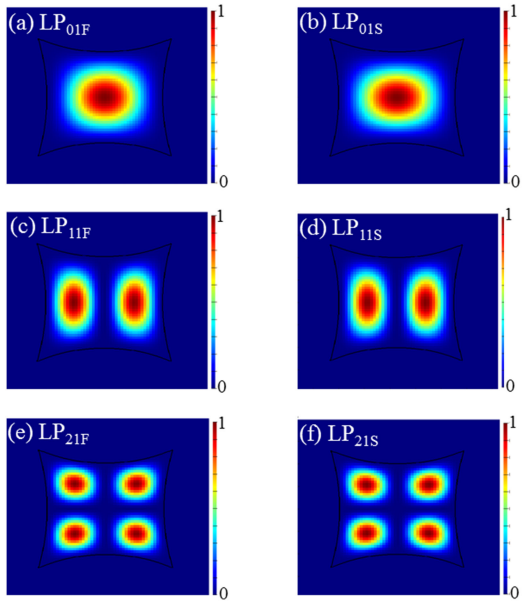

Fig. 2. Calculated six polarization modes in the tellurite HBMOF. (a) $LP_{01\mathrm{F}}$, (c) $LP_{11\mathrm{F}}$, and (e) $LP_{21\mathrm{F}}$ along the fast axis, and (b) $LP_{01\mathrm{S}}$, (d) $LP_{11\mathrm{S}}$, and (f) $LP_{21\mathrm{S}}$ along the slow axis.

incident light. At 1062.7 nm three modes were emitted, namely, LP_{01}, LP_{11}, and LP_{21}. Calculated by a commercial software (Lumerical MODE Solution) using the full-vectorial mode solver technology, six polarization modes in all were obtained, which were denoted as $LP_{01\mathrm{F}}$, $LP_{11\mathrm{F}}$ and $LP_{21\mathrm{F}}$ along the fast axis, and $LP_{01\mathrm{S}}$, $LP_{11\mathrm{S}}$ and $LP_{21\mathrm{S}}$ along the slow axis, as shown in Fig. 2.

Fig. 3(a) shows the calculated modal effective refractive indices (n_{eff}) of $LP_{01\mathrm{F}}$, $LP_{01\mathrm{S}}$, $LP_{11\mathrm{F}}$, $LP_{11\mathrm{S}}$, $LP_{21\mathrm{F}}$ and $LP_{21\mathrm{S}}$. We can see that n_{eff} of the polarization modes along the slow axis are larger than those along the fast axis, LP_{01} being the largest while LP_{21} being the smallest. The GVD of six polarization modes are presented in Fig. 3(b), all locating in the deep normal dispersion regime of the tellurite HBMOF at 1062.7nm. The nonlinear coefficients (γ) of $LP_{01\mathrm{F}}$, $LP_{01\mathrm{S}}$, $LP_{11\mathrm{F}}$,

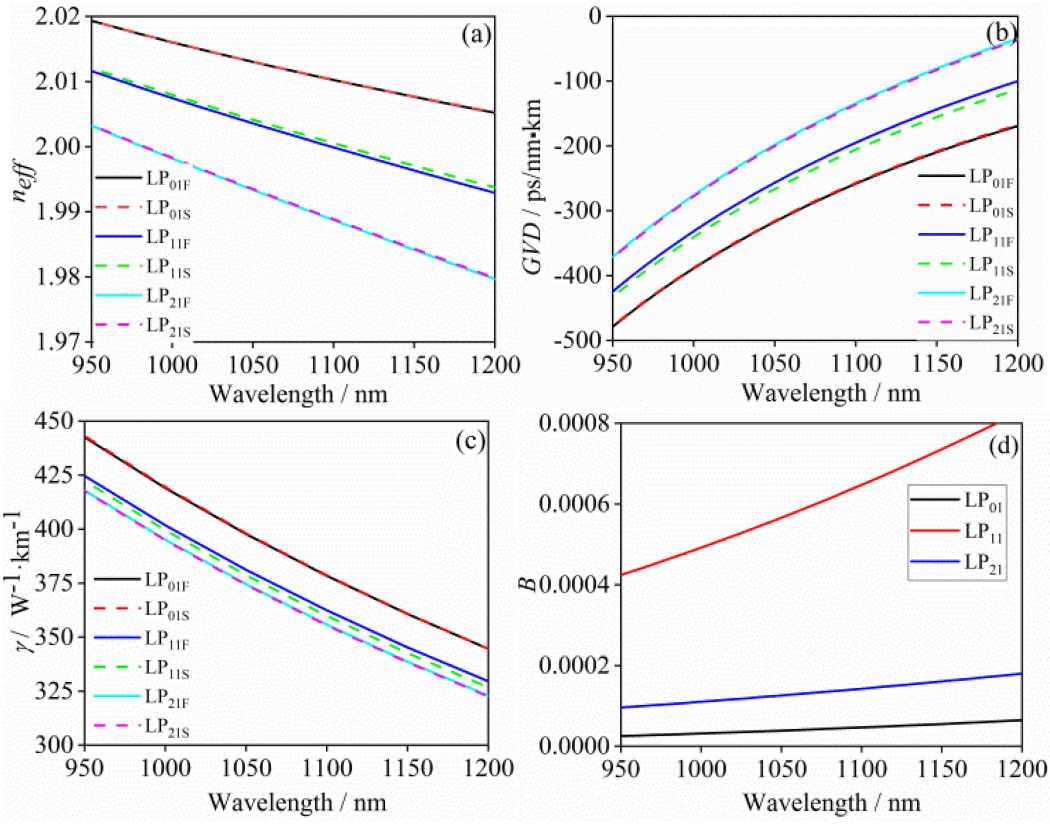

Fig. 3. (a) Calculated modal effective refractive indices. (b) Calculated GVD. (c) Calculated nonlinear coefficients. (d) Calculated modal birefringence.

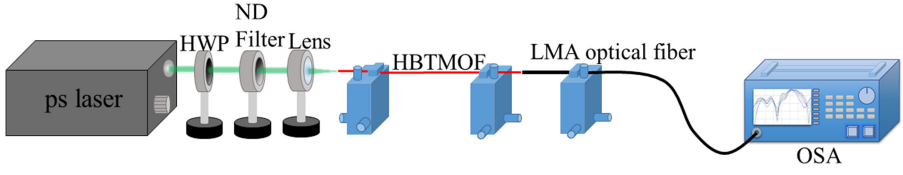

Fig. 4. Experimental setup for investigating XPMI in a 30 cm tellurite HBMOF.

LP_{11S}, LP_{21F} and LP_{21S} are calculated based on the nonlinear-index coefficient of tellurite glass ($n_2 = 5.9 \times 10^{-19}$ m^2W^{-1}), as shown by Fig. 3(c). The n_{eff} difference of each two corresponding polarization modes induced a modal birefringence $B = |n_s - n_f|$, and the respective value for LP_{01}, LP_{11} and LP_{21} is calculated to be $\sim 4.2 \times 10^{-5}$, 5.9×10^{-4} and 1.3×10^{-4} at 1062.7 nm, as shown by Fig. 3(d). The high modal birefringence feature provides a good platform for our investigation on XPMI.

3. Experimental Results and Discussion

A picosecond laser with a center wavelength of ~1062.7 nm, a pulse width of ~15 ps and a repetition rate of ~80 MHz was used for investigating XPMI in a 30 cm tellurite HBMOF, as shown in Fig. 4. A half-wave plate (HWP) was inserted to adjust the polarization state of the pump to the axis of the tellurite HBMOF. The pump was coupled into the tellurite HBMOF core by an

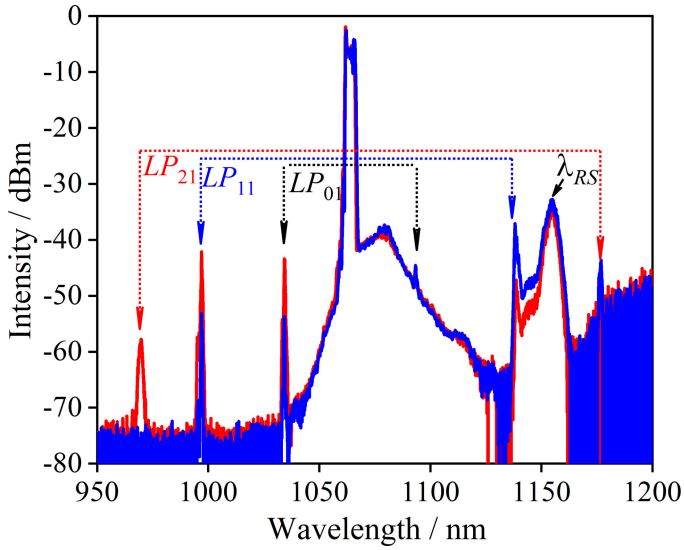

Fig. 5. Output spectra of the tellurite HBMOF at the average pump power of 300 mW with the orthogonal polarization state of the Stokes and anti-Stokes sidebands.

TABLE 2
Average Pump Power, Average Output Power and Peak Input Power of the Tellurite HBMOF With the Pump

Average pump power / mW	300	470	600	920
Average output power / mW	4.6	5.2	5.6	6.1
Peak input power / W	3.8	4.3	4.7	5.1

aspheric objective lens with a focal length of 6.24 mm and a numerical aperture (NA) of 0.40 (NEWPORT, F-LA11, 510∼1550 nm). The output signal was butt-coupled into a large-mode-area (LMA) optical fiber with a coupling efficiency over 95%. The LMA optical fiber was connected to an optical spectrum analyzer with a measurement range of 350∼1200 nm (OSA, Yokogawa) to record the spectra.

Firstly, in order to confirm the generation of XPMI, the polarization state of the output sidebands was experimentally analyzed. A polarization beam splitter (PBS) and a polarization controller were used at the output end of the tellurite HBMOF, and HWP was adjusted to maintain the most obvious output MI effect at the average pump power of 300 mW. Fig. 5 shows the output spectra, where the peak at 1154 nm (λ_{RS}) belonged to the stimulated Raman scattering (SRS) and the Raman shift corresponded well with [Ref. 32]. When the polarization controller and PBS were in the position to obtain the largest Stokes sidebands, the anti-Stokes sidebands were observed in their minimum state (blue line). After the polarization controller turned around 90°, the Stokes sidebands turned weak and LP_{01}, LP_{21} disappeared. The anti-Stokes sidebands became the largest while the Stokes sidebands were reduced to the smallest (red line). We can see that the polarization state of the Stokes and anti-Stokes sidebands was orthogonal, which accorded with [14], verifying that XPMI was generated in this tellurite HBMOF.

Then, the polarization controller and PBS were removed for the experimental investigation concerning the evolution of XPMI spectrum with HWP's adjustment of the polarization state of the pump. The azimuth of the HWP was first fixed at the occurrence of the maximal XPMI, and according to [14], at this moment the linear polarization of the pump was at 45° to the principal axes of the tellurite HBMOF. Table 2 shows the average pump power, average output power and peak input power of the tellurite HBMOF. The average pump power was measured by a power meter after the ND filter and the average output power was measured by OSA. The peak power

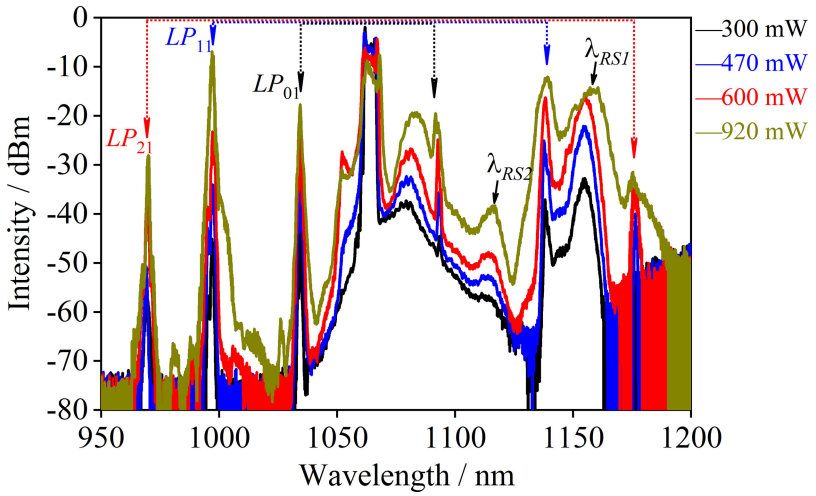

Fig. 6. Output spectra of the tellurite HBMOF at the average pump power of 300, 470, 600 and 920 mW with the pump linear polarization at 45° to the principal axes.

TABLE 3
Center Wavelength and Wavelength Shift from the Pump at the Average Pump Power of 920 mW

	λ_{Stokes} /nm	$\lambda_{Anti\text{-}Stokes}$ /nm	Stokes shift/cm^{-1}	Anti-Stokes shift /cm^{-1}
Fundamental mode (LP_{01})	1092	1035	253	252
Higher-order mode (LP_{11})	1138	997	623	621
Higher-order mode (LP_{21})	1179	996	928	931

was calculated based on the Gauss pump. When the pump pulse transmitted in the fiber core, a power of only 0.06 dB (0.3 m $\times$ 0.2 dB/m) was lost, and a power of less than 5% was lost at the output end of the tellurite HBMOF. Thus the average output power was treated approximately the same as the average input power, and based on it, the peak input power launched into the tellurite HBMOF was calculated. In the experimental setup, the coupling efficiency was low due to several possible reasons: the spot after the lens was larger than the core; the numerical aperture (NA) of the fiber and the lens did not match well, and the surface of the tellurite HBMOF was not smooth.

Fig. 6 shows the output spectra of the tellurite HBMOF at the average pump power of 300, 470, 600 and 920 mW. In contrast to the previous XPMI investigation in optical fibers which are mainly single pair induced by the fundamental mode [1], [3]–[5], [13]–[16], a three-pair XPMI was obtained in our experiment, induced respectively by LP_{01}, LP_{11} and LP_{21}. For each mode, with the increase of the pump power, its Stokes sidebands slightly redshifted while the anti-Stokes sidebands slightly blueshifted. Table 3 shows the center wavelengths of the Stokes and the anti-Stokes, and their shifts from the pump at 920 mW. During the experimental process, the light source and the space light coupling system suffered from minor instability due to the external environment, thus the frequency shift of the Stokes and anti-Stokes from the pump were slightly different. Together with the observation of the three-pair XPMI, SRS was obtained at 1154 nm (λ_{RS1}) and 1114 nm (λ_{RS2}) and the Raman shift corresponded well with Ref. 32. In the Stokes region, SRS and XPMI overlapped, which induced the Stokes sidebands of the three-pair XPMI to grow wider but turn weaker compared with the anti-Stokes sidebands. The observation of an increased number of XPMI is primarily due to three reasons. Firstly, tellurite HBMOFs have high nonlinear material indices which can improve MI generation. Secondly, they have high refractive-index difference between the core and cladding which can emit multiple modes. Finally, the multiple modes satisfied multiple phase matching conditions. In this work, three emitted modes, LP_{01}, LP_{11} and LP_{21}, satisfied three phase matching conditions and generated three pairs of XPMI. To the

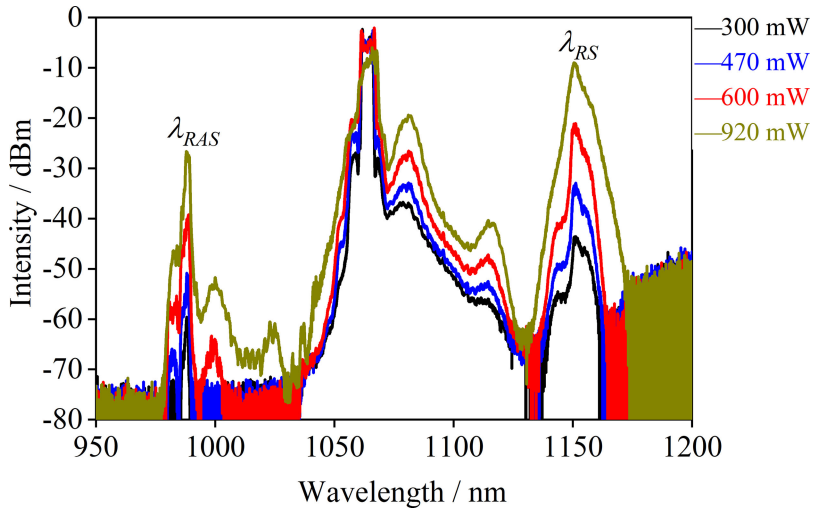

Fig. 7. Output spectra of the tellurite HBMOF at the average pump power of 300, 470, 600 and 920 mW with the pump linear polarization at 0° to the principal axes.

TABLE 4
Average Pump Power, Average Output Power and Peak Input Power of the Tellurite HBMOF With the Pump Linear Polarization at 0° to the Principal Axes

Average pump power / mW	300	470	600	920
Average output power / mW	5.1	5.7	6.2	6.8
Peak input power / W	4.3	4.8	5.2	5.7

best of our knowledge, this is the first report on the observation of multi-pair XPMI in optical fibers, which open new applications for multi-wavelength fiber amplifiers and all-optical modulators.

When the HWP turned 45° or -45°, the linear polarization of the pump was at 0° to the slow or fast axis. The three-pair XPMI disappeared and the output spectra at the average pump power of 300, 470, 600 and 920 mW were the same, as presented in Fig. 7. Table 4 lists the average pump power, average output power and peak input power of the tellurite HBMOF. It is to be noted that at this azimuth of the HWP, only SRS was obtained with the Raman Stokes (λ_{RS}) and Raman anti-Stokes (λ_{RAS}), implying that right now the linear polarization of the pump coincided to the principal axes of the tellurite HBMOF and that the interactions of the linearly polarized modes disappeared. The Raman Stokes peaks were located at 1154 nm and 1114 nm, and the Raman anti-Stokes peaks at 985 nm and 996 nm, the Raman shift of which corresponded well with the Raman gain of TBLZ glass [32]. When the HWP turned another 45°, the three-pair XPMI reappeared, and with the continual rotation of 45°, the disappearance and reappearance of the three-pair XPMI alternated regularly.

Fig. 8 shows the XPMI gain (G) of LP_{01}, LP_{11}, and LP_{21} at the average pump power of 920 mW, which was calculated using the following equations [2]:

$$[(K - \Omega/v_{g1})^2 - f_1][(K - \Omega/v_{g2})^2 - f_2] = C^2 \quad (1)$$

$$g(\Omega) = 2\mathrm{Im}(K) \quad (2)$$

Y coordinate is the relative intensity of the gain and X coordinate is the Stokes shift from the pump. We can see that each mode has a different XPMI gain curve because of the different n_{eff}, GVD and γ. The maximum XPMI gain occurred respectively at 252 cm^{-1}, 622 cm^{-1} and 930 cm^{-1}, which corresponded well to the three experimental wavelengths of XPMI in Table 3.

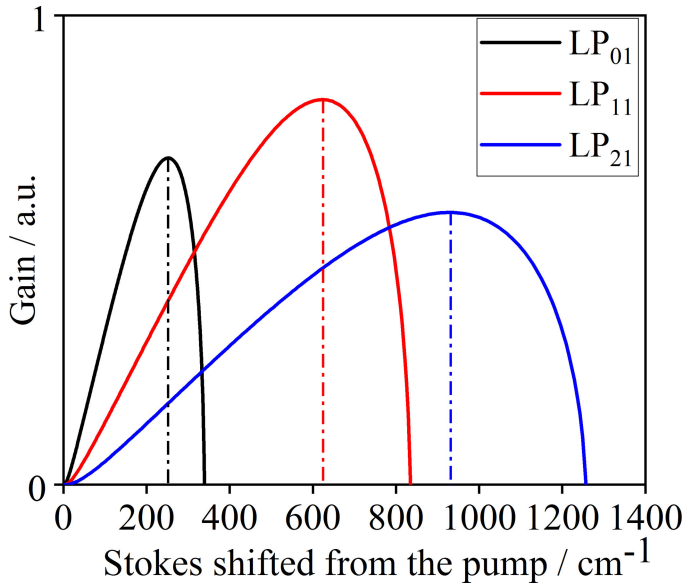

Fig. 8. Calculated XPMI gain of LP_{01}, LP_{11} and LP_{21} at the average pump power of 920 mW.

4. Conclusion

In summary, we designed and fabricated a tellurite HBMOF based on the TBLZ glass. At 1062.7 nm three modes were emitted, namely, LP_{01}, LP_{11} and LP_{21}, and altogether six polarization modes were calculated along the principal axes of the tellurite HBMOF. The modal birefringence of the three modes was on the order of $>10^{-5}$, which provides a good platform for the XPMI observation. Using a picosecond laser as the pump source, a three-pair XPMI was obtained in the deep normal dispersion regime of the tellurite HBMOF, and it disappeared/reappeared regularly with each 45° rotation of the HWP. The XPMI gain induced by the three modes was calculated, which corresponded well to the experimental results. This observation of multi-pair XPMI generation in the optical fiber provide reference for the development of multi-wavelength fiber amplifiers and all-optical modulators.

Acknowledgment

The authors thank the Liao Ning Revitalization Talents Program.

References

[1] A. Hasegawa and F. Tappert, "Transmission of stationary nonlinear optical pulses in dispersive dielectric fibers. I. Anomalous dispersion," *Appl. Phys. Lett.*, vol. 23, pp. 142–144, 1973.
[2] G. P. Agrawal, *Nonlinear Fiber Optics*, 5th ed., San Francisco, CA, USA: Academic, 2013.
[3] K. Tai, A. Hasegawa, and A. Tomita, "Observation of modulational instability in optical fibers," *Physical Rev. Lett.*, vol. 56, 1986, Art. no. 135.
[4] F. Amrani, B. Kibler, P. Grelu, S. Wabnitz, S. Trillo, and G. Millot, "Cross-phase modulational instability induced by Raman scattering in highly birefringent fiber," *Opt. Lett.*, vol. 38, no. 24, pp. 5327–5330, 2013.
[5] S. Junaid, K. Schaarschmidt, M. Chemnitz, M. Chambonneau, S. Nolte, and M. A. Schmidt, "Tailoring modulation instabilities and four-wave mixing in dispersion-managed composite liquid-core fibers," *Opt. Exp.*, vol. 28, no. 3, pp. 3097–3106, 2020.
[6] R. T. Murray, E. J. R. Kelleher, S. V. Popov, A. Mussot, A. Kudlinski, and J. R. Taylor, "Synchronously pumped photonic crystal fiber-based optical parametric oscillator," *Opt. Lett.*, vol. 37, no. 15, pp. 3156–3158, 2012.
[7] P. Franco, F. Fontana, I. Cristiani, M. Midrio, and M. Romagnoli, "Self-induced modulational-instability laser," *Opt. Lett.*, vol. 20, no. 19, pp. 2009–2011, 1995.
[8] M. N. Islam, S. P. Dijaili, and J. P. Gordon, "Modulation-instability-based fiber interferometer switch near 1.5 μm," *Opt. Lett.*, vol. 13, no. 6, pp. 518–520, 1988.

[9] J. G. Rarity, J. Fulconis, J. Duligall, W. J. Wadsworth, and P. St. J. Russell, "Photonic crystal fiber source of correlated photon pairs," *Opt. Exp.*, vol. 13, no. 2, pp. 534–544, 2005.
[10] J. A. Slater *et al.*, "Microstructured fiber source of photon pairs at widely separated wavelengths," *Opt. Lett.*, vol. 35, no. 4, pp. 499–501, 2010.
[11] S. Lefrancois *et al.*, "Fiber four-wave mixing source for coherent anti-Stokes raman scattering microscopy," *Opt. Lett.*, vol. 37, no. 10, pp. 1652–1654, 2012.
[12] T. Gottschall *et al.*, "Fiberbased source for multiplex-CARS microscopy based on degenerate four-wave mixing," *Opt. Exp.*, vol. 20, no. 11, pp. 12004–12013, 2012.
[13] J. I. Gersten, R. R. Alfano, and M. Belic, "Combined stimulated raman scattering and continuum self-phase modulations," *Phys. Rev. A*, vol. 21, no. 4, pp. 1222–1224, 1980.
[14] A. Kudlinski *et al.*, "Simultaneous scalar and cross-phase modulation instabilities in highly birefringent photonic crystal fiber," *Opt. Exp.*, vol. 21, no. 7, pp. 8437–8440, 2013.
[15] H. Zhang, M. Bigot-Astruc, P. Sillard, G. Millot, B. Kibler, and J. Fatome, "Multiple spatial and wavelength conversion operations based on a frequency-degenerated intermodal four-wave mixing process in a graded-index 6-LP few-mode fiber," *Appl. Opt.*, vol. 59, no. 18, pp. 5497–5505, 2020.
[16] A. Armaroli and S. Trillo, "Modulational instability due to cross-phase modulation versus multiple four-wave mixing: The normal dispersion regime," *J. Opt. Soc. Am. B*, vol. 31, no. 3, pp. 551–558, 2014.
[17] R. R. Alfano and S. L. Shapiro, "Emission in the region 4000 to 7000 Å via four-photon coupling in glass," *Phys. Rev. Lett.*, vol. 24, no. 11, pp. 584–588, 1970.
[18] R. R. Alfano, *The Supercontinuum Laser Source*, 3rd ed., New York, NY, USA; Berlin, Germany: Springer, 2016.
[19] J. E. Rothenberg, "Modulational instability for normal dispersion," *Phys. Rev. A*, vol. 42, no. 1, pp. 682–685, 1990.
[20] P. D. Drummond, T. A. B. Kennedy, J. M. Dudley, R. Leonhardt, and J. D. Harvey, "Cross-phase modulational instability in high-birefringence fibers," *Opt. Commun.*, vol. 78, no. 2, pp. 137–142, 1990.
[21] G. Millot, P. Tchofo Dinda, E. Seve, and S. Wabnitz, "Modulational instability and stimulated raman scattering in normally dispersive highly birefringent fibers," *Opt. Fiber Technol.*, vol. 7, no. 3, pp. 170–205, 2001.
[22] G. Millot and S. Wabnitz, "Nonlinear polarization effects in optical fibers: Polarization attraction and modulation instability," *J. Opt. Soc. Am. B*, vol. 31, no. 11, pp. 2754–2768, 2014.
[23] T. Yajima, K. Yushihara, C. B. Harris, and S. Shionoya, *Ultrafast Phenomena VI*, eds, New York, NY, USA; Berlin, Germany: Springer, 1988.
[24] T. Tanemura and K. Kikuchi, "Unified analysis of modulational instability induced by cross-phase modulation in optical fibers," *J. Opt. Soc. Amer. B*, vol. 20, no. 12, pp. 2502–2514, 2003.
[25] S. F. B. Mazhar and R. R. Alfano, "Modulation instability induced by cross-phase modulation of transient stimulated raman scattering and self-phase modulation in calcite," *Opt. Lett.*, vol. 45, no. 11, pp. 3167–3170, 2020.
[26] J. Li, K. Chiang, and C. Li, "Modulation instability in collinear three-core optical fibers," *J. Opt. Soc. Amer. B*, vol. 34, no. 12, pp. 2467–2477, 2017.
[27] E. O. Alves, W. B. Cardoso, and A. T. Avelar, "Modulation instability in a nonlinear oppositely directed coupler with saturable nonlinearities and high-order effects," *J. Opt. Soc. Amer. B*, vol. 33, no. 6, pp. 1134–1142, 2016.
[28] J. Li, H. Xu, T. Sun, S. Pei, and H. Ren, "Effects of intramode nonlinearity and intramode nonlinearity on modulation instability in randomly birefringent two-mode optical fibers," *Opt. Commun.*, vol. 415, no. 1, pp. 74–81, 2018.
[29] T. Cheng, S. Tanaka, T. Tuan, T. Suzuki, and Y. Ohishi, "All-optical dynamic photonic bandgap control in an all-solid double-clad tellurite photonic bandgap fiber," *Opt. Lett.*, vol. 42, no. 12, pp. 2354–2357, 2017.
[30] M. Belal *et al.*, "Mid-infrared supercontinuum generation in suspended core tellurite microstructured optical fibers," *Opt. Lett.*, vol. 40, no. 10, pp. 2237–2240, 2015.
[31] T. Cheng *et al.*, "Highly efficient second-harmonic generation in a tellurite optical fiber," *Opt. Lett.*, vol. 44, no. 19, pp. 4686–4689, 2019.
[32] A. Mori, "Tellurite-based fibers and their applications to optical communication networks," *J. Ceram. Soc. Jpn.*, vol. 116, no. 1358, pp. 1040–1051, 2008.
[33] T. Cheng, S. Li, T. Suzuki, and Y. Ohishi, "Cascaded cross-phase modulation instability in the normal dispersion regime of a birefringent tellurite microstructured optical fiber," *IEEE Photon. J.*, vol. 10, 2018, Art. no. 7101508.